JNRD
JOURNAL OF NATURAL RESOURCES AND DEVELOPMENT

JOURNAL OF NATURAL RESOURCES AND DEVELOPMENT

Research article

Analysis of Droughts in Southwest Indian Ocean Countries using SPI and SPEI and their Relationship with Global SST

Pulak Guhathakurta and Nilesh Wagh

India Meteorological Department, Pune, Maharashtra, 411005, India
Corresponding author. E-mail: pguhathakurta@rediffmail.com

Article history

Received 17.06.2021
Accepted 02.11.2022
Published 20.06.2022

Keywords

Drought index
Standardized precipitation index
Standardized precipitation evapotranspiration index
Potential evapotranspiration
Global SST teleconnection
Temporal correlation

Abstract

Drought is a continuous period of dry weather. It is one of the most severe problems for human societies and ecosystems caused by a deficiency in rainfall in an affected region. The most affected are tropical monsoon-dependent agricultural regions, including Africa. Drought indices like Standardized Precipitation Index (SPI) and Standardized Precipitation Evapotranspiration Index (SPEI) are useful and well-accepted drought indices representing the magnitude and severity of drought at a particular location by identifying the water stresses. In the present study, the SPI and the SPEI are used to understand the drought severity in eight coastal and one landlocked country in the southwest Indian Ocean. It is observed that the maximum rainfall amount received by these countries is during the period December to March (D-J-F-M). To understand drought magnitude and severity, we have calculated four months cumulative SPI and SPEI for the months with the maximum rainfall amount. Furthermore, the decadal rainfall variability has been assessed to precisely identify multi-decadal dry and wet phases in the study regions. In addition, the relationship between both SPI and SPEI of the nine countries with global Sea Surface Temperature, various El Nino and with dipole mode indices of Indian Ocean Dipole has been analyzed to understand different teleconnections responsible for the drought.

1. Introduction

The Southwest Indian Ocean (SWIO) region is characterized by several islands grouped into states (Comoros, Madagascar, Mauritius, and Seychelles), and several island territories (La Reunion, etc.). The countries that share most of their borders with the ocean (Mozambique, South Africa, Tanzania, etc.), termed as coastal countries, are considered the area of study in our present analysis. These countries are different in terms of their climatic properties. Very few studies have been done in the past, including studies on drought occurrence over the Indian Ocean region (Bouchard C et al. 2019). The major natural disasters in the SWIO region are caused by tropical cyclones, floods, and droughts (SWIO-RAFI, 2017). On average, the SWIO basin experiences nine to eleven tropical cyclones annually (Muthige M S et al. 2018). These tropical cyclones cause landfall along the eastern coast of southern Africa and are responsible for flooding in SWIO region countries (Muthige M S et al. 2018). Droughts are one of the most significant concerns for the SWIO region due to the high risk of crop or livestock loss (SWIO-RAFI, 2017). Droughts can have severe long-lasting socio-economic impacts as the lack of rainfall results in poor agricultural production, water scarcity, and reduction in trade associated with the agricultural sector.

Drought indices are an essential tool to represent a drought's magnitude and severity and compare the duration and extent across different climatic regions. The Standardized Precipitation Index (SPI) is the normalization of precipitation anomalies, widely accepted to represent meteorological, agricultural or hydrological drought if computed for different time periods (M. Svoboda et a. 2012). However, SPI only considers precipitation as accumulated precipitation can be compared across other climatic regions or locations. Variables or parameters used to describe drought conditions include precipitation, temperature, streamflow, groundwater and reservoir levels, soil moisture, etc. To overcome these limitations, a new drought index, the Standardized Precipitation Evapotranspiration Index (SPEI), was developed by Vicente-Serrano et al. (2010). Instead of normalizing precipitation, SPEI normalizes the accumulated climatic water balance represented by the difference between precipitation and potential evapotranspiration. Hence, SPEI includes a broader measure of climatic conditions while providing a more comprehensive measure of water availability. Therefore, we can say that the SPEIis an alternate version of the commonly used SPI. SPEI is a measure of water availability in terms of climatic water balance as it includes Potential Evapotranspiration (PET). SPEI is a better drought index than SPI since the drought indices that use evapotranspiration data to monitor drought have shown better results than precipitation-based drought indices (Narasiman et al. 2005).

Sea surface temperatures (SSTs) variations impact means seasonal rainfall anomalies over Africa to some extent, and the SSTs influence the climate predictability of most of Africa (Rowell. 2013; Giannini A. 2010). Linkage of Southern African summer rainfall variability with the El Niño–Southern Oscillation (ENSO) phenomenon has been investigated by Mo and White (1985), Lindesay (1988), Ropelewski and Halpert (1987, 1989, 1996), Shinoda and Kawamura (1996), Rocha and Simmonds (1997), Richard et al. (2001). Atlantic and Indian Ocean SSTs largely influence African rainfall due to their effect on large-scale circulation (Ting et al. 2009). Ujeneza & Abiodun (2014) have used SPI and SPEI to identify drought incidences over Southern African countries and have a strong teleconnection with SST over the tropical pacific.

In this study, we have tried to analyze the drought events based on SPI and SPEI and the sensitivity of the drought index by including PET to measure the magnitude and severity of drought. This study is done for nine Indian Ocean countries by comparing SPI and SPEI along with their correlation with global SST. In the

primary part of the study, we have computed the monthly rainfall climatology of all nine countries for classifying the year's wet season. SPI and SPEI are then computed for the cumulative period of December-January-February-March, which is the most rain-producing period for all nine countries. We have compared moderate, severe, and extreme drought years derived by both SPI and SPEI for months of D-J-F-M. In the second part of the study, we have used the monthly mean SSTs for El Nino 1+2, Nino 3, Nino 3.4, Nino 4, and Nino West along with dipole mode indices of IOD and Subtropical Indian Ocean Dipole (SIOD) regions and have derived their correlations with SPI and SPEI to show their relationship with droughts in SWIO countries. A temporal correlation is also done between global SST and SPI and SPEI for months of DJFM to identify SST regions with positive feedback for drought in these countries.

2. Selection of Study Region

For this study, we have selected eight coastal countries and a group of islands in South West Indian Ocean region, namely Comoros, Madagascar, Mauritius, Mozambique, Reunion, Seychelles, South Africa, Tanzania, and one landlocked country viz. Lesotho which is surrounded by South Africa (Figure 1). These are coastal SWIO countries, which receive most of their rainfall during the months of December to March. The rain received during the month of April also plays a vital role in droughts in some of these countries (Hua et al., 2016).

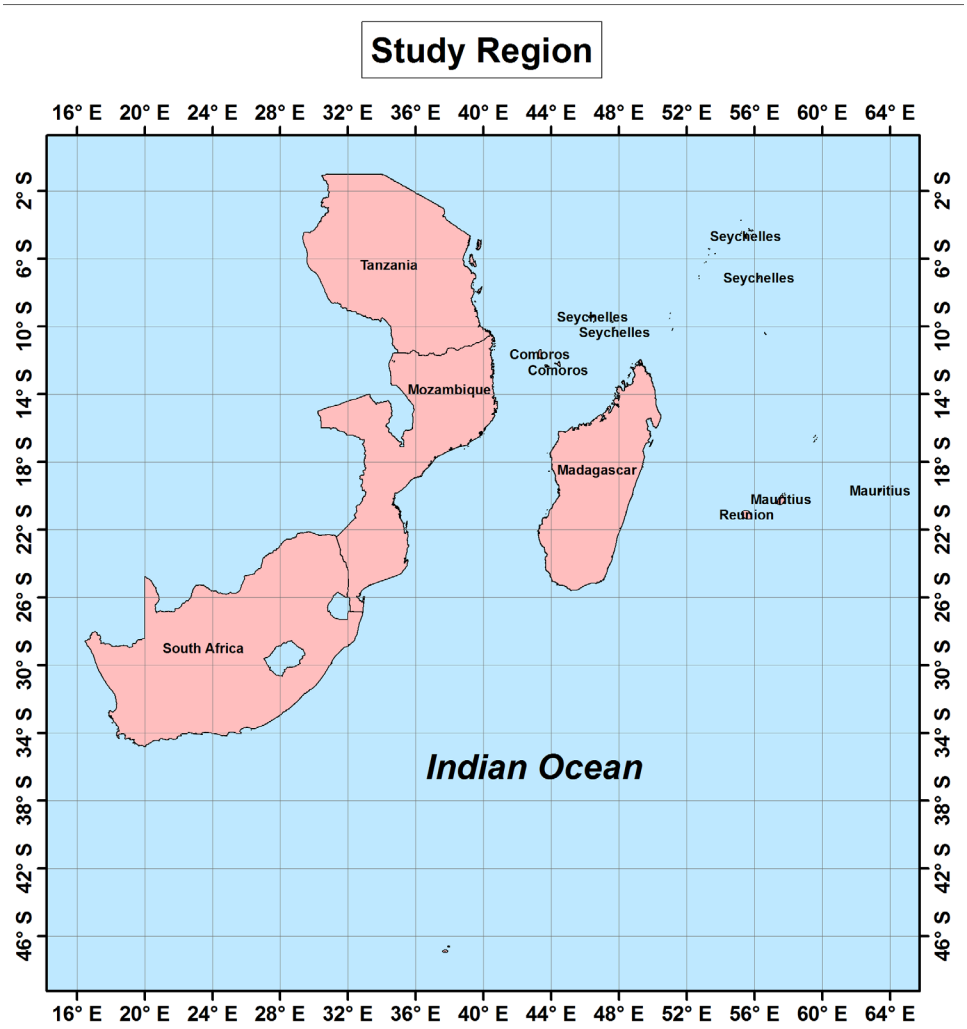

Figure 1: Study Region in the southwest Indian Ocean

We have also used SST data of well-known regions to study the teleconnections with the drought occurrences in the study region. SSTs play a vital role in the rainfall patterns of these coastal countries. To study the influence of SST on rainfall patterns in these countries, we have selected various SST regions in the Indian and Pacific Oceans. The Indian Ocean Dipole (IOD) is defined by the difference in SST between two areas (or poles, hence a dipole), a western pole (50E-70E, 10S-10N) in the Arabian Sea (western Indian Ocean) and an eastern pole (90E-110E, 10S-0N) in the eastern Indian Ocean south of Indonesia (Saji et al. 1999). The well-known Niño regions are Niño 1+2 (EQ-10S, 90W-80W), Niño 3 (5N-5S, 150W-90W), Niño 3.4 (5N-5S, 170W-120W) and Niño 4 (5N-5S, 160E-150W). Another less known Niño region is called Niño West (15N-EQ, 130E-150E) (Yoshida C et al. 2016). The Subtropical Indian Ocean Dipole (SIOD) is a feature caused by SST oscillations where the southwest part of the Indian Ocean, i.e., south of Madagascar, is warmer and then colder than the eastern part of the Indian Ocean, i.e., off Australia (Behera S K et al. 2001). During the positive phase of SIOD, SSTs in the south-western part of the Indian Ocean, i.e., south of Madagascar, are warmer than normal, and SSTs in the eastern part of the Indian Ocean, i.e., off Australia, are colder than normal. This causes the above normal rainfall over Central and South Africa, also causing increased rainfall during summer months over south-eastern Africa (Behera S K et al. 2001). On the other hand, during the negative phase of SIOD, the SST in the south-western part is cooler, and in the eastern part, SSTs are warmer (Behera S K et al. 2001). SIOD generally evolves during December – January, peaks in February, is followed by a decay in subsequent two months, and finally dies down during May – June. The SIOD Index is computed from the SST anomaly difference between the western (55E-65E, 37S-27S) and eastern (90E-100E, 28S-18S) the Indian Ocean.

3. Data and Methodology

3.1. Data

Two types of datasets viz. CRU TS v4.04 and COBE SST2 were mainly utilized for the analysis in this study. Monthly rainfall, maximum and minimum temperature datasets for the period 1901-2019 of all countries (dataset for Mauritius and Reunion was available for period 1951-2019) are taken from the Climate Research Unit (CRU) data portal of the University of East Anglia (UEA). We have used the CRU TS v4.04 version of the dataset, which provides historical datasets derived from observational data and provides quality-controlled temperature and rainfall data. The global gridded monthly Sea Surface Temperature (SST) COBE-SST2 dataset for the period 1901-2019 data provided by NOAA's Earth System Research Laboratory's Physical Science Laboratory (ESRL-PSL) data portal. We have also used the COBE SST2 dataset to calculate the monthly mean SST time series for Nino, IOD, and SIOD regions. Data source links are provided in Table 1.

Table 1: Table 1. Details of Various Datasets used in Study

Parameter	Sources (URL)	Time Period	Time Scale
Rainfall	https://crudata.uea.ac.uk/cru/data/hrg/	1901-2019	Monthly
Temperature	https://crudata.uea.ac.uk/cru/data/hrg/	1901-2019	Monthly
Global SST	https://psl.noaa.gov/data/gridded/data.cobe2.html	1901-2019	Monthly

3.2. Drought Indices

SPI and SPEI for all nine countries are calculated, and results are discussed separately for each country. The drought years obtained from our study were also supported by the historical drought record maintained at EM-DAT (https://public.emdat.be/data) in most cases (Masih I et al., 2014). The detailed information about these drought indices is discussed below.

3.2.1. SPI

A rainfall deficit over a period at a specific location could lead to various degrees of drought conditions. The drought definition or concept may differ from one place to another as there is a significant variation in rainfall among different regions (Wilhite D A et al. 1985). World Meteorological Organization (WMO) recommends adopting the Standardized Precipitation Index (SPI) to monitor the severity of drought events for a more effective assessment of the drought phenomena (WU Man-chi 2013). At a specific geographical location, SPI, in simple terms, is a normalized index that represents the probability of occurrence over a long-term reference period of observed rainfall amount compared to the rainfall anomaly. Negative SPI values represent dry conditions, whereas positive SPI values indicate wet conditions. SPI values can be quantified over different time scales (e.g., 3, 6, 12, or 24-month rainfall), which is helpful in the analyses of drought impact on various water resource needs. For example, SPI-3 measures dry/wet conditions over a 3-month period, the anomalies of which impact primarily on soil water conditions and agricultural produce; while SPI for six or more months can indicate hydrological drought, as prolonged droughts can give rise to shortfalls in groundwater, streamflow, and new water storage in reservoirs (Gupta A K et al. 2011). The significant advantage of SPI is that it only needs a single parameter for computation. SPI can also be compared across regions of different climatic zones (WU Man-chi 2013). Detailed information about the methodology and applications of SPI is available at WMO (2012).

3.2.2. SPEI

The principle of Standardized Precipitation Evapotranspiration Index (SPEI) is almost similar to Standardized Precipitation Index (SPI) (Vicente-Serrano et al. 2015), but it uses both precipitation and potential evapotranspiration (PET) to determine drought. Thus, unlike the SPI, the SPEI captures the main impact of increased temperatures on water demand (Vicente-Serrano et al., 2015). Similar to the SPI, the SPEI can also be calculated for different timescales ranging from 1 to 48 months. At longer timescales (>~18 months), the SPEI has been shown to correlate with the self-calibrating Palmer Drought Severity Index (sc-PDSI) (Vicente-Serrano et al. 2015). The Hargreaves method can be used to estimate PET in case only temperature and precipitation data are available. In this simplified approach, variables that can affect PET, such as wind speed, surface humidity, and solar radiation, are not accounted for (Vicente-Serrano et al., 2015). Another method, viz Penman-Monteith is widely used for the computation of PET, but it involves more parameters, and it is most challenging to get the values in real-time monitoring. In the present study, we have used the Hargreaves method to estimate monthly PET values from maximum and minimum temperature data. As mentioned earlier, the climatic water balance equation (Precipitation - PET) is used to calculate SPEI (Vicente-Serrano et al., 2015). A log-logistic distribution is used to fit the monthly time series of climatic water balance to obtain SPEI values.

3.3. Drought Category Classification

To show a comparative representation of range (magnitude) and category (severity) of droughts (Table 2) by both SPI and SPEI we have sampled out some of the drought years derived by both SPI and SPEI. The classification is based on SPI and SPEI shown in Table 2 for each category of drought. Monthly time series of temperature and precipitation are used to calculate SPI and SPEI. A standard gamma distribution for SPI and log-logistic distribution for SPEI is used to fit the time-series data. Then it has been transformed to a standard normal distribution with zero mean and one standard deviation. Only precipitation is used to calculate SPI, whereas both temperature and precipitation are considered to estimate SPEI. Initially, potential evapotranspiration is calculated using temperature by Hargreaves method, and later a climatic water balance is taken to determine SPEI for each year. For this study, we have computed both SPI and SPEI over a four-month cumulative period for December to March (D-J-F-M). The analysis is being done separately for all the nine counties, and accordingly, results have been discussed.

Table 2: Drought Classification based on SPI or SPEI value

Category	Range
Extremely Wet	2.00 or more
Severely Wet	1.50 to 1.99
Moderately Wet	1.00 to 1.49
Mildly Wet	0.00 to 0.99
Mildly Dry	0.00 to -0.99
Moderately Dry	-1.00 to -1.49
Severely Dry	-1.50 to -1.99
Extremely Dry	-2.00 or less

3.4. Correlation of SPEI and SPI with SST

The correlation function is generally used to identify the statistical relationship between different random variables in terms of spatial or temporal distance (Storch H V et al. 1999). Here, high resolution gridded dataset of monthly mean SSTs (COBE SST2) is used to calculate monthly series (1901-2019) for SST regions like Nino 1+2, Nino 3, Nino 3.4, Nino 4, Nino West, along with IOD and SIOD. Further, a relationship between SPI of all nine countries and SSTs of IOD, SIOD, Nino 1+2, Nino 3, Nino 3.4, Nino 4, and Nino West regions are analyzed using correlation coefficient for D-J-F-M months. Similar computation has been done for SPEI SSTS. Correlation coefficients are calculated at 95% (indicated with * following correlation values for significant values in Table 5) and 99% (marked with ** following correlation values for significant values in Table 5) significance level with df(N-2)=117 for Comoros, Lesotho, Madagascar, Mozambique, Seychelles, South Africa, Tanzania and df(N-2)=67 for Mauritius, Reunion. A temporal correlation is also done between global SST and SPI and SPEI to understand their relationship other than the aforementioned SST regions for D-J-F-M months and identify SST regions responsible for the droughts in SWIO countries.

4. Results

4.1. Monthly Rainfall Climatology

Monthly rainfall climatology has been analyzed to determine the months that contribute maximum rainfall amount for each country and determine the period to be considered rainy/wet seasons (Figure 2). We have also computed the percent of annual rainfall for each of the twelve months to see the rainfall contribution of each month (Table 3). The results for monthly rainfall climatology analysis for each country are discussed below.

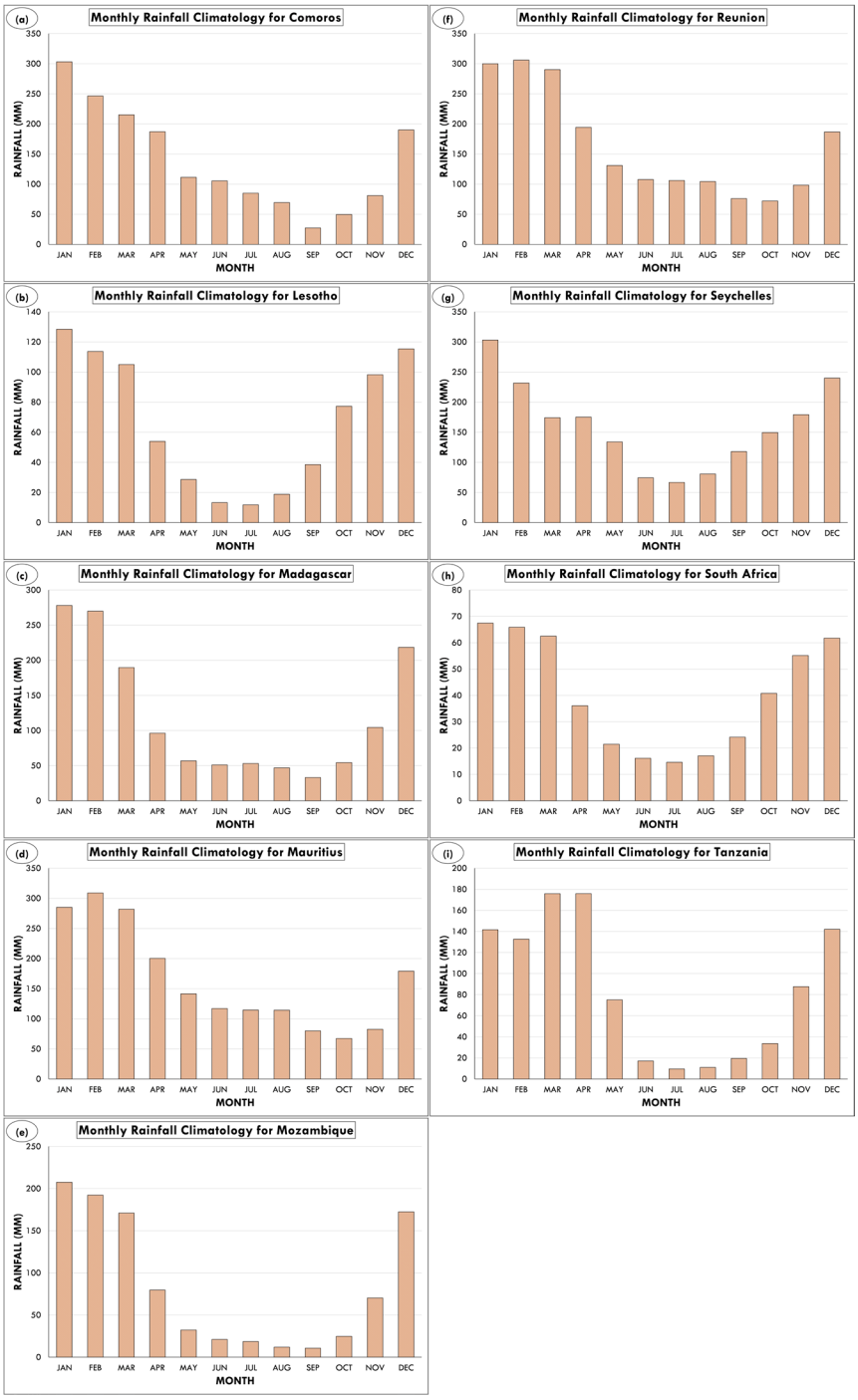

Figure 2: Monthly Rainfall Climatology for Each Country

Table 3: Percent of Annual Rainfall for Each Country

YEAR	COM	LES	MAD	MAU	MOZ	REU	SAF	SEY	TAN
JAN	**18.14**	**16.00**	**19.15**	**14.46**	**20.50**	**15.21**	**13.97**	**15.74**	**13.87**
FEB	**14.75**	**14.16**	**18.59**	**15.67**	**19.00**	**15.52**	**13.64**	**12.03**	**12.99**
MAR	**12.88**	**13.08**	**13.06**	**14.29**	**16.89**	**14.71**	**12.94**	**9.04**	**17.22**
APR	**11.20**	6.72	6.63	**10.16**	7.87	**9.85**	7.47	**9.09**	**17.22**
MAY	6.66	3.56	3.91	7.17	3.19	6.64	4.44	6.95	7.35
JUN	6.31	1.65	3.52	5.93	2.08	5.46	3.34	3.86	1.67
JUL	5.09	1.46	3.65	5.81	1.83	5.38	3.02	3.46	0.93
AUG	4.15	2.34	3.23	5.79	1.18	5.29	3.54	4.19	1.07
SEP	1.63	4.80	2.28	4.05	1.05	3.85	5.00	6.12	1.90
OCT	2.96	9.62	3.74	3.41	2.44	3.65	8.44	7.76	3.29
NOV	4.85	**12.23**	7.19	4.19	6.94	4.98	**11.42**	**9.30**	8.58
DEC	**11.38**	**14.37**	**15.04**	**9.08**	**17.03**	**9.47**	**12.78**	**12.46**	**13.91**

4.1.1. Comoros

As shown in the monthly rainfall climatology chart (Fig 2a) for Comoros, maximum rainfall of around 300 mm (more than 18% of annual rainfall) occurs in January, followed by February (246.4mm) and March (215.1mm). The cumulative rainfall contributed by D-J-F-M months was more than 950 mm, about 57% of the annual rainfall amount (Table 3).

4.1.2. Lesotho

Fig 2b shows the monthly rainfall climatology for Lesotho. January is the most rain-producing month with an average rainfall of nearly 130 mm (16% of annual rainfall) followed by December (115mm) with 14.4% of annual rainfall, February (114 mm) with 14.2% of annual rainfall, and March (105 mm) with 13.1% of annual rainfall. The cumulative rainfall contributed by D-J-F-M months is the rainiest period as the average rainfall for this period is more than 640 mm, which is about 57% of the annual rainfall amount (Table 3).

4.1.3. Madagascar

As seen in the monthly rainfall climatology chart (Fig 2c) for Madagascar, we can identify the D-J-F-M months as the wettest period since cumulative rainfall of these months contributed more than 950 mm, representing about 65% of the annual rainfall amount (Table 3). It is noticeable that Madagascar receives the highest rainfalls (278 mm) of the year in January, corresponding to more than 19 % of annual rainfall, followed by February (270 mm), December (218 mm), and March (190 mm).

4.1.4. Mauritius

As seen in the monthly rainfall climatology chart (Fig 2d) for Mauritius, February shows maximum rainfall values (309 mm) with a share of around 16 % followed by January (285 mm) and March (282 mm). The Fourth-highest rainfall-producing month is April, with around 10% of annual rainfall, while December contributes around 9% of annual rainfall. Cumulative rainfall by the months of J-F-M-A is more than 1070 mm, about 54% of the annual rainfall amount (Table 3). While cumulative rainfall contributed by the months of D-J-F-M is more than 1050 mm, which is about 53% of the annual rainfall.

4.1.5. Mozambique

As seen in Mozambique's monthly rainfall climatology chart (Fig 2e), the highest rainfall is received in January (207 mm), followed by February, March, and December. The cumulative rainfall contributed by the months of D-J-F-M is more than 740 mm and is about 73% of the annual rainfall amount since it represents the rainy period (Table 3).

4.1.6. Reunion

Fig. 2f shows the monthly rainfall climatology for Reunion. It is noticeable that February receives the highest rainfall (mm) in a year for Reunion. January and March receive slightly less rainfall than February. Cumulative rainfall contributed by the months of J-F-M-A is around 1090 mm, about 55% of annual rainfall (Table 3). While cumulative rainfall contributed by D-J-F-M months is more than 1080 mm, which is about 54% of the annual rainfall.

4.1.7. Seychelles

As seen in the monthly rainfall climatology chart (Fig 2g) for Seychelles, D-J-F-M months can be considered the wettest period as the cumulative rainfall contributed in this period is more than 940 mm, which is about 49% of the annual rainfall amount. However, almost similar cumulative rainfall was contributed by N-D-J-F months (Table 3). It is noticeable that January receives the highest rainfall in a year for Seychelles.

4.1.8. South Africa

The monthly rainfall climatology chart (Fig 2h) for South Africa shows that January is the wettest month for this country, followed by February, March, and December. We can consider D-J-F-M months as the wettest period where that cumulative rainfall contributed is more than 250 mm, which is about 53% of the annual rainfall amount (Table 3).

4.1.9. Tanzania

Fig 2i shows the monthly rainfall climatology for Tanzania. It is noticeable that March receives the highest rainfall within a year, while April has the second-highest rainfall values over Tanzania. Cumulative rainfall contributed by J-F-M-A is more than 620 mm, which is about 61% of the annual rainfall amount (Table 3). However, cumulative rainfall contributed by D-J-F-M is about 57% of the annual rainfall amount.

Thus we can see that for most countries, D-J-F-M months contributed most of the annual rainfall, and this period can be considered the wettest period. Rainfall received during this period has a significant contribution to the agricultural, water, and other sectors involving the economy of these countries. Analysis of SPI or SPEI conditions for this period is thus considered.

4.2. Decadal Rainfall Variability

Decadal rainfall variability has been analyzed using the percent departure of each decade for all nine countries. Figure 3 shows the percent departure charts for months of D-J-F-M. The alternating sequence of multi-decadal periods having frequent wet and dry phases is also clearly noticed. The results for decadal rainfall variability for each country are discussed below.

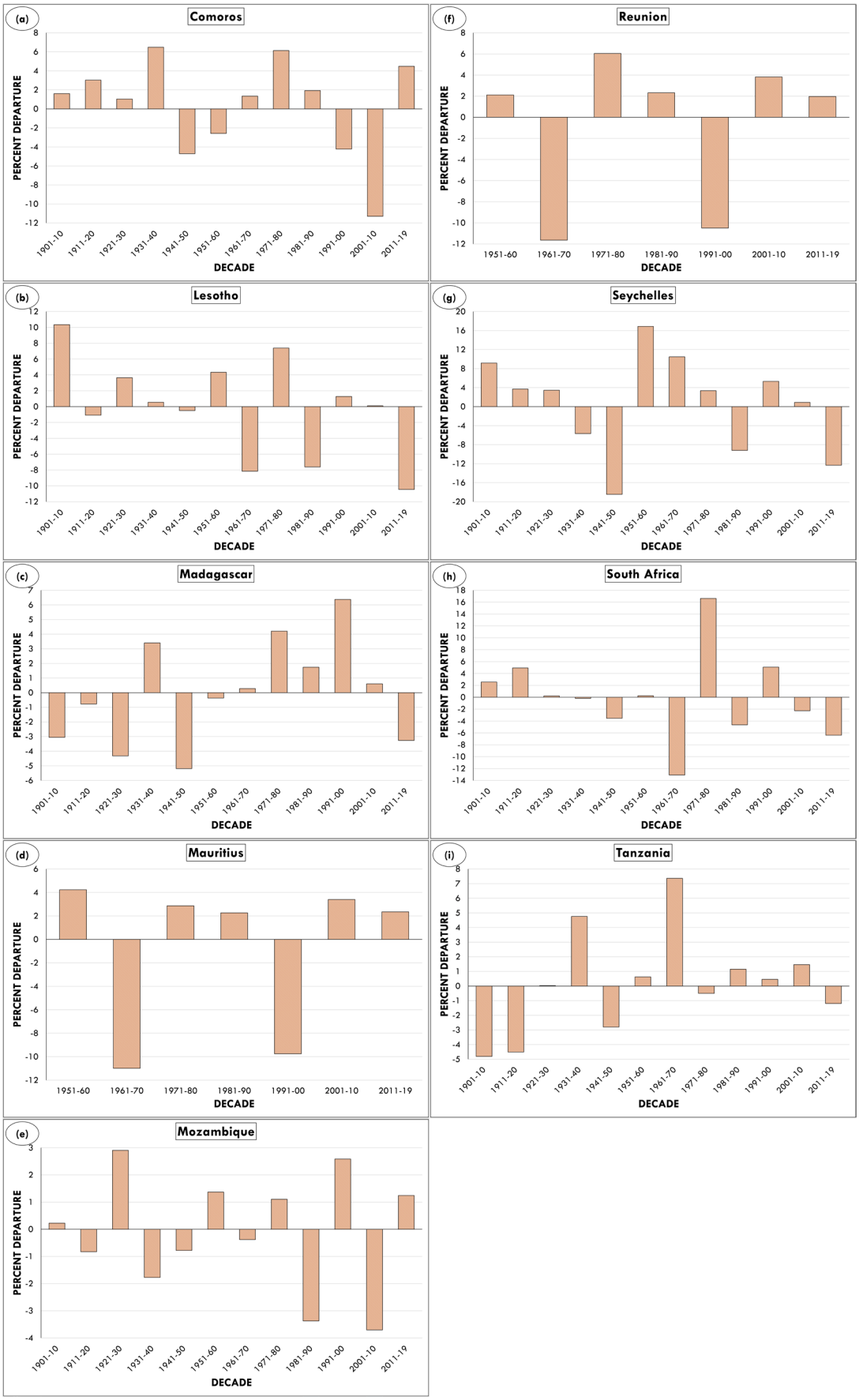

Figure 3: Decadal Rainfall Percent Departure for Months of D-J-F-M.

4.2.1. Comoros

As seen in Comoros's decadal rainfall percent departure chart, we can identify the multi-decadal wet and dry phases (Fig. 3a). The first four decades during 1901-40 were wet for months of D-J-F-M. Further, the next two decades during 1941-60 were dry periods which were followed by a wet period for three decades during 1961-90. The decades during 1991-2010 were dry periods which were followed by a wet phase for a current decade until 2019. It is noticeable that 1931-40 was the wettest and 2001-2010 was the driest decade for Comoros.

4.2.2. Lesotho

As seen in Lesotho's decadal rainfall percent departure chart (Fig. 3b), decades during 1901-10, 1921-40, 1951-60, 1971-80, 1991-2010 were periods of wet phases. At the same time, dry phases were seen in decades during 1911-20, 1941-50, 1961-70, 1981-90, and the current decade until 2019. It is noticeable that 1901-10 was the wettest and 2011-2019 was the driest decade of the century for Lesotho.

4.2.3. Madagascar

Madagascar's decadal rainfall percent departure chart does not show any clear multi-decadal nature of wet and dry phases (Fig. 3c). The first three decades during 1901-30 were dry for months of D-J-F-M. Further, the next decade during 1931-40 were wet periods followed by dry periods for two decades during 1941-60. The following five decades during 1961-2010 were wet periods followed by a dry phase for the current decade until 2019. It is noticeable that 1991-2000 was the wettest and 1941-50 was the driest decade of the century for Madagascar.

4.2.4. Mauritius

For Mauritius, rainfall data from 1951 onwards was available. Mauritius's decadal percent departure chart (Fig. 3d) shows only two decades during 1961-70 and 1991-2000 as dry phase, whereas the rest of the decades were periods of wet phase. It can be seen that 1951-60 was the wettest and 1961-70 was the driest decade of the last half-century for Mauritius.

4.2.5. Mozambique

As seen in Mozambique's decadal rainfall percent departure chart, we can delineate multi-decadal wet and dry phases (Fig. 3e). Mozambique has experienced an alternating sequence of decades for wet and dry phases. During 1901-10, 1921-30, 1951-60, 1971-80, 1991-2000, and the current decade until 2019 were periods of wet phases. In comparison, dry phases were seen in decades during 1911-20, 1931-50, 1961-70, 1981-90, and 2001-10. It is noticeable that 1921-30 was the wettest and 2001-10 was the driest decade of the century for Mozambique.

4.2.6. Reunion

For Reunion, rainfall data from 1951 onwards was available. The decadal percent departure chart for Reunion shows that only two decades during 1961-70 and 1991-2000 were dry phases, whereas the rest of the decades were periods of wet phases. It can be seen that 1971-80 was the wettest and 1961-70 was the driest decade of the last half century for Reunion.

4.2.7. Seychelles

As seen in the decadal rainfall percent departure chart for Seychelles, we can see some multi-decadal wet and dry phases (Fig. 3g). The first three decades during 1901-30 were wet for months of D-J-F-M. Further, the next two decades during 1931-50 were dry periods which were followed by a wet period for three decades during

1951-80. The next decade during 1981-90 was the dry period which was followed by a wet phase for the next two decades during 1991-2010. The current decade until 2019 is a period of dry phase. It is noticeable that 1951-60 was the wettest and 1941-50 was the driest decade of the century for Seychelles.

4.2.8. South Africa

The decadal rainfall percent departure chart for South Africa is shown in Fig. 3h. Decades during 1901-20, 1971-80, 1991-2000 were periods of wet phases. In contrast, dry phases were seen in decades during 1941-50, 1961-70, 1981-90, and 2001-19. In addition, decades during 1921-40 and 1951-60 were periods of near-neutral phase. It is noticeable that 1921-30 was the wettest and 2001-10 was the driest decade of the century for South Africa.

4.2.9. Tanzania

As seen in Tanzania's decadal rainfall percent departure chart, we can delineate some multi-decadal wet and dry phases (Fig. 3i). The first two decades during 1901-20 were wet for months of D-J-F-M. Further, the next decade during 1921-30 was a near-neutral phase period, followed by a wet period for the next decade during 1931-40. The decade during 1941-50 was the dry period which was followed by a wet phase for decades during 1951-70. The next decade during 1971-80 was a period of dry phase which followed by three wet decades during 1981-2010. The current decade until 2019 is in the wet phase. It is noticeable that 1961-70 was the wettest and 1901-10 was the driest decade of the century for Tanzania.

4.3. Temporal Variability of SPI and SPEI

The SPI and SPEI have shown the multivariate nature of droughts and have been useful to determine the severity and magnitude of droughts in the SWIO region. These can be the most useful tool to monitor and predict the same conditions at the current stage. However, it is seen that SPEI gives a more accurate representation of drought as it uses climatic water balance from both temperature and precipitation while SPI, which uses only precipitation to standardize it and to normalize the conditions, may give a somewhat representation of drought. Based on the SPI and SPEI values, we have identified the years for each of the nine countries for the moderate, severe, and extreme drought conditions cumulative for the period D-J-F-M, respectively, shown in Table 4. Similarly, Figure 4 shows the SPI and SPEI time series for all nine countries cumulative for period D-J-F-M.

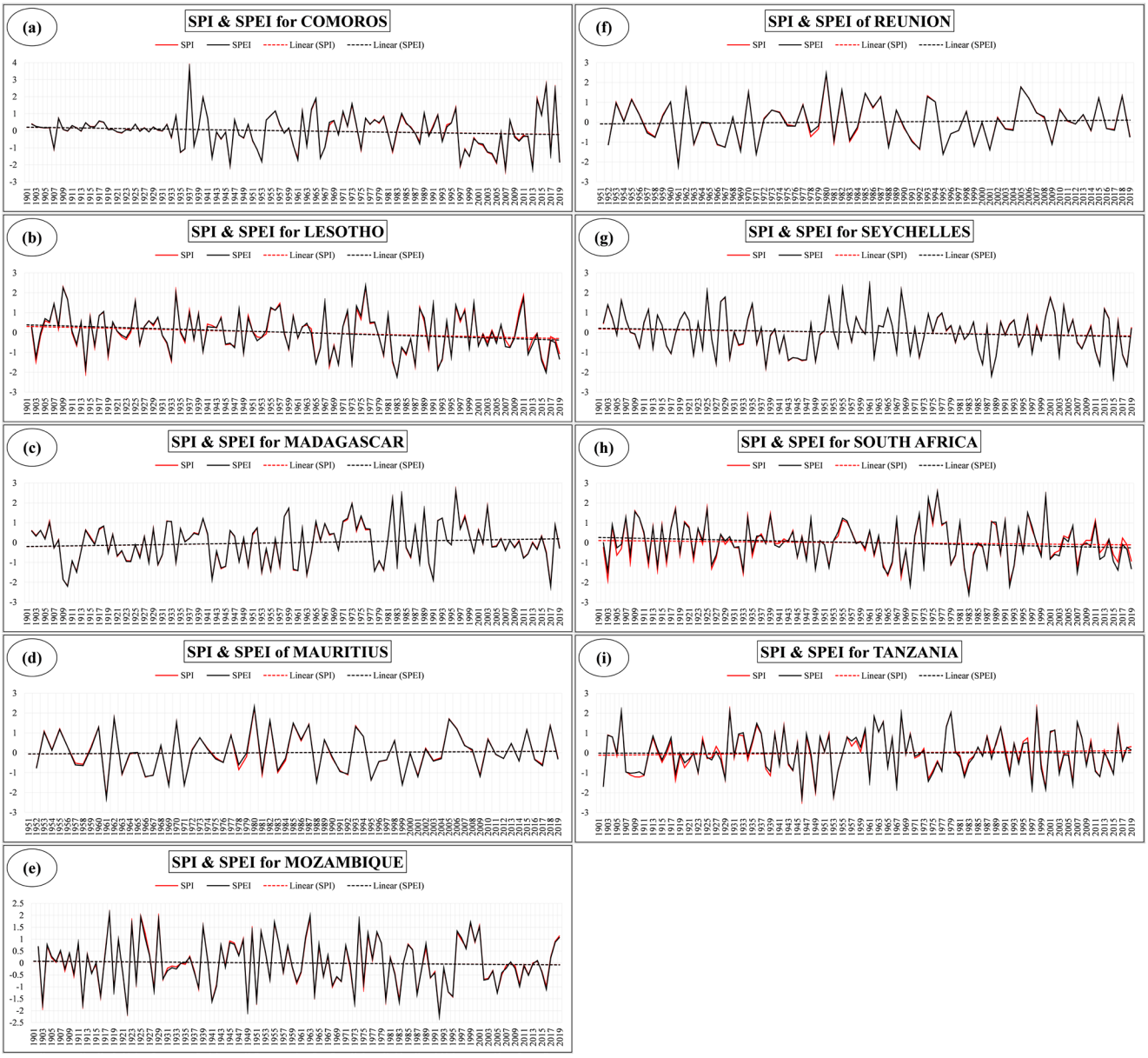

Figure 4: SPI and SPEI Time Series for Months of D-J-F-M

Table 4: Drought Magnitude and Years based on SPI and SPEI for Months of D-J-F-M

Ctry.	Index	Moderate	Severe	Extreme
Comoros	SPEI	1938, 1951, 1960, 1963, 1967, 1988, 1993, 2001, 2002, 2010	1907, 1935, 1936, 1952, 1975, 1982, 1998, 1999, 2003, 2004, 2017	1942, 1946, 1953, 1961, 1966, 1997, 2005, 2007, 2013, 2019
	SPI	1938, 1951, 1960, 1963, 1967, 1988, 1993, 2001, 2002, 2010	1907, 1935, 1936, 1952, 1975, 1982, 1998, 2003, 2004, 2017	1942, 1946, 1953, 1961, 1966, 1997, 1999, 2005, 2007, 2013, 2019
Lesotho	SPEI	1912, 1916, 1926, 1932, 1940, 1945, 1946, 1947, 1959, 1966, 1969, 1984, 1990, 1999, 2001, 2003, 2005, 2007, 2008, 2013	1903, 1919, 1933, 1949, 1980, 1982, 1985, 1993, 1995, 2012, 2015,2019	1914, 1965, 1968, 1970, 1973, 1983, 1987, 1992, 2016
	SPI	1912, 1916, 1926, 1932, 1940, 1945, 1946, 1947, 1959, 1966, 1969, 1984, 1990, 1999, 2001, 2008, 2012	1903, 1919, 1933, 1949, 1980, 1985, 1993, 1995, 2015, 2019	1914, 1965, 1968, 1970, 1973, 1982, 1983, 1987, 1992, 2016
Madagascar	SPEI	1911, 1919, 1921, 1923, 1924, 1926, 1931, 1934, 1948, 1979, 1986, 2011, 2012, 2016	1912, 1928, 1930, 1944, 1945, 1950, 1953, 1955, 1957, 1960, 1961, 1978, 1980, 1983, 1988, 1990	1909, 1910, 1942, 1963, 1991, 2017
	SPI	1911, 1921, 1923, 1924, 1926, 1928, 1931, 1948, 1964, 1979, 1986, 1988, 2000, 2011, 2012	1912, 1930, 1934, 1944, 1945, 1950, 1955, 1957, 1960, 1961, 1978, 1980, 1983, 1990	1909, 1910, 1942, 1953, 1963, 1991, 2017
Mauritius	SPEI	1952, 1957, 1958, 1978, 1981, 1983, 1991, 2017	1963, 1966, 1967, 1988, 1992, 1995, 2001, 2009	1961, 1969, 1971, 1999
	SPI	1952, 1957, 1958, 1978, 1983, 1991, 2017	1963, 1966, 1967, 1981, 1988, 1992, 1995, 2001, 2009	1961, 1969, 1971, 1999
Mozambique	SPEI	1924, 1930, 1942, 1954, 1960, 1966, 1968, 1969, 1970, 1975, 1990, 2002, 2003, 2010, 2012	1916, 1919, 1928, 1938, 1964, 1987, 1994, 1995, 2005, 2016	1903, 1912, 1922, 1941, 1949, 1951, 1973, 1980, 1983, 1992
	SPI	1910, 1924, 1930, 1942, 1954, 1960, 1966, 1969, 1970, 1990, 2002, 2003, 2010, 2016	1916, 1919, 1928, 1938, 1964, 1968, 1975, 1987, 1994, 1995, 2005	1903, 1912, 1922, 1941, 1949, 1951, 1973, 1980, 1983, 1992
Reunion	SPEI	1957, 1958, 1978, 1981, 1983, 1991, 1996, 2019	1952, 1963, 1966, 1967, 1969, 1988, 1992, 1999, 2001, 2009	1961, 1971, 1995
	SPI	1958, 1978, 1983, 1991, 1996, 2019	1952, 1963, 1966, 1967, 1969, 1981, 1988, 1992, 1999, 2001, 2009	1961, 1971, 1995
Seychelles	SPEI	1910, 1913, 1916, 1924, 1932, 1933, 1936, 1954, 1985, 1994, 2007, 2008, 2011	1917, 1922, 1930, 1941, 1943, 1944, 1945, 1946, 1947, 1949, 1962, 1967, 1970, 1972, 1989, 1997, 2003, 2017	1927, 1938, 1986, 1988, 2012, 2015, 2018
	SPI	1910, 1913, 1916, 1924, 1932, 1933, 1936, 1954, 1980, 1985, 1994, 2008, 2011	1917, 1922, 1930, 1941, 1943, 1944, 1945, 1946, 1947, 1949, 1962, 1967, 1970, 1972, 1989, 1997, 2003, 2017	1927, 1938, 1986, 1988, 2012, 2015, 2018
South Africa	SPEI	1908, 1912, 1916, 1922, 1927, 1945, 1947, 1962, 1966, 1980, 1984, 1990, 1999, 2001, 2002, 2003, 2012, 2013, 2015	1903, 1914, 1926, 1933, 1949, 1952, 1964, 1973, 1979, 1982, 1987, 1993, 2016, 2019	1965, 1968, 1970, 1983, 1992, 2007
	SPI	1905, 1919, 1922, 1927, 1935, 1945, 1947, 1962, 1980, 1984, 1990, 1999, 2001, 2002, 2015, 2016, 2019	1908, 1912, 1914, 1916, 1926, 1949, 1952, 1964, 1966, 1973, 1979, 1982, 1987, 1993, 2007	1903, 1933, 1965, 1968, 1970, 1983, 1992
Tanzania	SPEI	1907, 1909, 1910, 1923, 1938, 1939, 1941, 1943, 1944, 1954, 1965, 1977, 1983, 1994, 1999, 2009, 2011	1908, 1911, 1918, 1929, 1961, 1974, 1975, 1982, 1992, 2003, 2012, 2015	1902, 1946, 1949, 1953, 1967, 1997, 2000, 2006
	SPI	1907, 1920, 1938, 1941, 1943, 1944, 1954, 1965, 1975, 1977, 1992, 1999, 2003, 2009, 2011, 2014	1908, 1909, 1910, 1911, 1918, 1923, 1929, 1939, 1961, 1974, 1982, 2006, 2012, 2015	1902, 1946, 1949, 1953, 1967, 1997, 2000

4.3.1. Comoros

Comoros SPI and SPEI time series for D-J-F-M show that there is a decreasing non-significant trend in both SPI and SPEI series (Fig. 4a). However, both SPI and SPEI are almost similar in nature, but there are differences in the years for different drought categories. SPI time series analysis shows 10% Moderate, 10% Severe, and 11% Extreme drought years; while based on SPEI, the time series analysis shows 10% Moderate, 11% Severe, and 10% extreme drought years in the period of last century (1901-2019) (Table 4).

4.3.2. Lesotho

SPI and SPEI time series for Lesotho for the period D-J-F-M show a decreasing non-significant trend in SPI and a significant decreasing trend in SPEI series (Fig. 4b). SPI time series analysis shows 17% Moderate, 10% Severe and 10% Extreme drought years; while based on SPEI, the time series analysis shows 20% Moderate, 12% Severe and 9% extreme drought years in the period of last century (1901-2019) (Table 4).

4.3.3. Madagascar

Madagascar SPI and SPEI time series for D-J-F-M show an increasing non-significant trend in SPI or SPEI series (Fig. 4c). The time-series analysis based on SPI shows 15% Moderate, 14% Severe, and 7% Extreme drought years. In comparison, the time series analysis based on SPEI shows 14% Moderate, 16% Severe, and 6% Extreme drought years during the period last half-century (1901-2019) (Table 4).

4.3.4. Mauritius

Mauritius SPI and SPEI time series for D-J-F-M show an increasing non-significant trend in SPI or SPEI series (Fig. 4d). The time-series analysis based on SPI shows 7% Moderate, 9% Severe, and 4% Extreme drought years. In comparison, the time series analysis based on SPEI shows 8% Moderate, 8% Severe and 4% Extreme drought years during the period last half-century (1951-2019) (Table 4).

4.3.5. Mozambique

Mozambique SPI and SPEI time series for D-J-F-M show a decreasing non-significant trend in SPI or SPEI series (Fig. 4e). The time-series analysis based on SPI shows 14% Moderate, 11% Severe and 10% Extreme drought years. In comparison, the time series analysis based on SPEI shows 15% Moderate, 10% Severe, and 10% Extreme drought years during the period last century (1901-2019) (Table 4).

4.3.6. Reunion

Reunion SPI and SPEI time series for D-J-F-M show an increasing non-significant trend in SPI or SPEI series (Fig. 4f). The time-series analysis based on SPI shows 6% Moderate, 11% Severe, and 3% Extreme drought years. In comparison, the time series analysis based on SPEI shows 8% Moderate, 10% Severe, and 3% Extreme drought years during the last half-century (1951-2019) (Table 4).

4.3.7. Seychelles

Seychelles SPI and SPEI time series for D-J-F-M show a decreasing non-significant trend in SPI or SPEI series (Fig. 4g). The time series analysis based on both SPI and SPEI shows 13% Moderate, 18% Severe, and 7% Extreme drought years during the period last century (1901-2019) (Table 4).

4.3.8. South Africa

South Africa SPI and SPEI time series for D-J-F-M show a decreasing non-significant trend in SPI or SPEI series (Fig. 4h). The time-series analysis based on SPI shows 17% Moderate, 15% Severe, and 7% Extreme drought years. In comparison, the time series analysis based on SPEI shows 19% Moderate, 14% Severe and 6% Extreme drought years during the period last century (1901-2019) (Table 4).

4.3.9. Tanzania

Tanzania SPI and SPEI time series for D-J-F-M show an increasing non-significant trend in SPI or SPEI series (Fig. 4i). The time-series analysis based on SPI shows 16% Moderate, 14% Severe and 7% Extreme drought years. In comparison, the time series analysis based on SPEI shows 17% Moderate, 12% Severe, and 8% Extreme drought years during the period last century (1901-2019) (Table 4).

4.4. Correlation of SPI and SPEI with Global SST

Here correlation coefficient (Table 5) and temporal correlation (Figure 5) of SPI and SPEI with SST show some noticeable and significant results, discussed below for each country separately.

Table 5: Correlation Coefficients between SPI and SPEI with IOD, SIOD and SSTs of Nino regions for D-J-F-M

Country	Index	Nino 1+2	Nino 3	Nino 3.4	Nino 4	Nino West	IOD	SIOD
Comoros	SPEI	-0.1170	-0.0717	-0.0570	-0.0530	-0.1384	-0.0371	**-0.1923***
	SPI	-0.1105	-0.0648	-0.0506	-0.0467	-0.1337	-0.0337	**-0.1906***
Lesotho	SPEI	**-0.3971****	**-0.4346****	**-0.4276****	**-0.4151****	0.0332	0.0659	0.0988
	SPI	**-0.3636****	**-0.4034****	**-0.3999****	**-0.3883****	0.0679	0.0674	0.0926
Madagascar	SPEI	0.0292	0.0094	-0.0049	-0.0103	-0.0246	0.2078*	0.0220
	SPI	0.0430	0.0269	0.0107	0.0036	-0.0224	0.2035*	0.0182
Mauritius	SPEI	-0.0604	-0.0174	-0.0113	-0.0199	0.0000	-0.0170	-0.0404
	SPI	-0.0537	-0.0155	-0.0101	-0.0179	0.0056	-0.0042	-0.0379
Mozambique	SPEI	**-0.2992****	**-0.4389****	**-0.4827****	**-0.4959****	**0.2127***	**0.2493****	**0.2392***
	SPI	**-0.2797****	**-0.4172****	**-0.4640****	**-0.4789****	**0.2230***	**0.2513****	**0.2373***
Reunion	SPEI	-0.0862	-0.0548	-0.0543	-0.0648	0.0360	-0.0337	-0.0071
	SPI	-0.0831	-0.0549	-0.0543	-0.0638	0.0372	-0.0216	-0.0041
Seychelles	SPEI	0.0065	0.0666	0.0682	0.0632	-0.2454**	0.0006	0.0347
	SPI	0.0205	0.0774	0.0771	0.0717	-0.2371*	0.0036	0.0328
South Africa	SPEI	**-0.4424****	**-0.5265****	**-0.5221****	**-0.5073****	0.0827	0.0615	0.1719
	SPI	**-0.3852****	**-0.4850****	**-0.4905****	**-0.4790****	0.1500	0.0659	0.1652
Tanzania	SPEI	0.1351	**0.2626****	**0.2944****	**0.3025****	**-0.2027***	0.0881	-0.1405
	SPI	0.1685	**0.2948****	**0.3228****	**0.3291****	-0.1725	0.0908	-0.1234

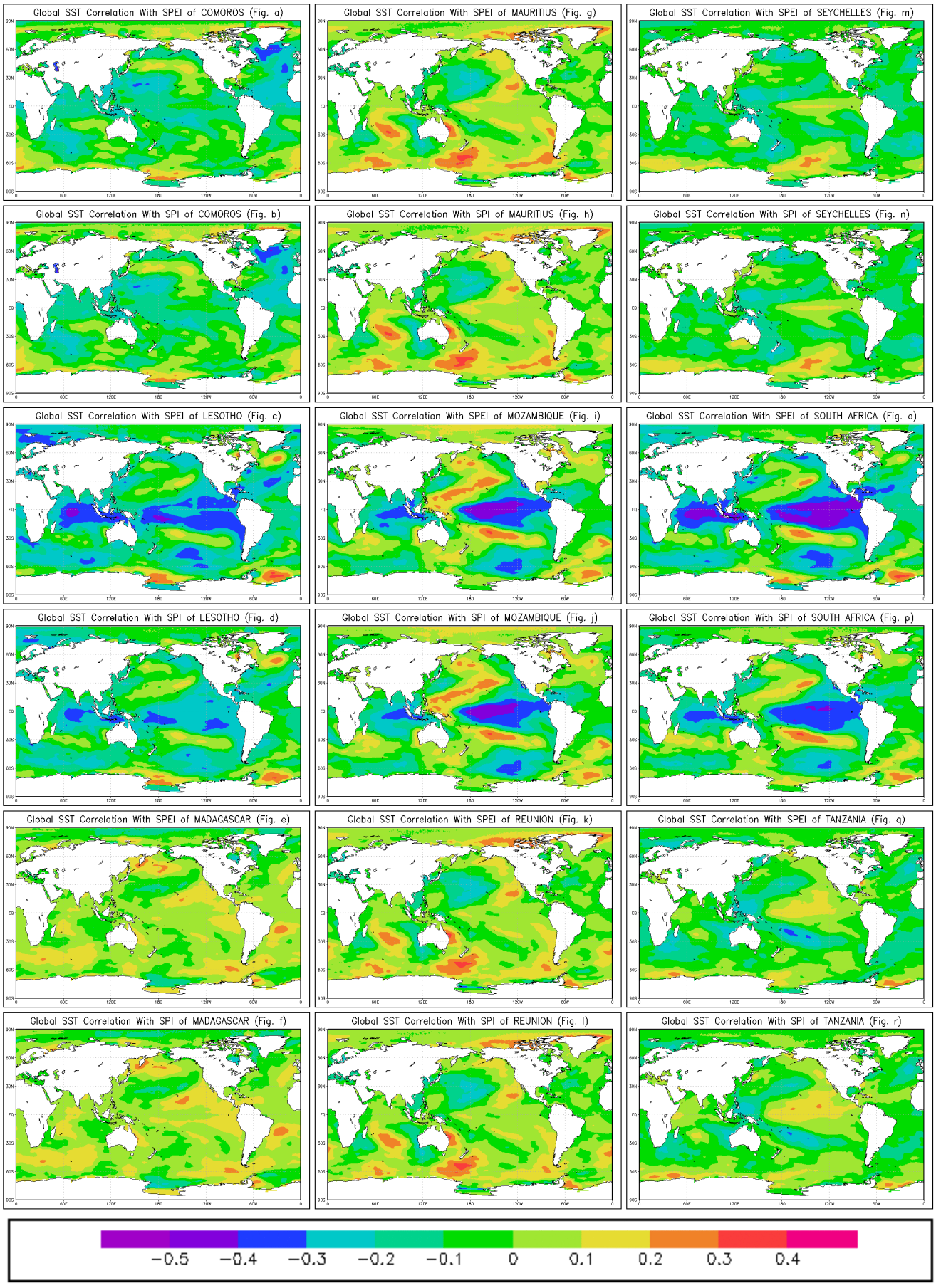

Figure 5: Global SST Correlation with SPI and SPEI for Months of D-J-F-M

4.4.1. Comoros

SPI and SPEI of Comoros have a significant negative relationship with SIOD and a non-significant negative relationship with IOD, Nino 1+2, Nino 3, Nino 3.4, Nino 4, and Nino West (Table 5). The temporal correlation with global SST indicates that Comoros's SPI and SPEI show a robust negative correlation with SSTs in North Atlantic Ocean and the Caspian Sea and a strong positive correlation with SSTs in the Antarctic Southern Ocean during months of D-J-F-M (Fig. 5a, 5b).

4.4.2. Lesotho

SPI and SPEI of Lesotho have a significant negative relationship with Nino 1+2, Nino 3, Nino 3.4, Nino 4 and a non-significant positive relationship with Nino West, IOD, SIOD (Table 5). The temporal correlation with global SST delineates that both SPI and SPEI of Lesotho show a strong negative correlation with SSTs in the Central and Extreme South Pacific Ocean and the Indian Ocean during months of D-J-F-M (Fig. 5c, 5d).

4.4.3. Madagascar

SPI and SPEI of Madagascar have a significant positive relationship with IOD and a non-significant relationship with Nino 1+2, Nino 3, Nino 3.4, Nino 4, Nino West, SIOD (Table 5). The temporal correlation with global SST delineates that both SPI and SPEI of Madagascar show a strong positive correlation with SSTs in a few small regions in the Pacific Ocean and South Atlantic Ocean during months of D-J-F-M (Fig. 5e, 5f).

4.4.4. Mauritius

SPI and SPEI of Mauritius have a non-significant positive relationship with Nino West and a non-significant negative relationship with Nino 1+2, Nino 3, Nino 3.4, Nino 4, IOD, SIOD (Table 5). The temporal correlation with global SST delineates that both SPI and SPEI of Mauritius show a strong negative correlation with SSTs in North Atlantic Ocean and the Caspian Sea during months of D-J-F-M (Fig. 5g, 5h).

4.4.5. Mozambique

SPI and SPEI of Mozambique have a significant positive relationship with Nino West, IOD, SIOD and a significant negative relationship with Nino 1+2, Nino 3, Nino 3.4, Nino 4 (Table 5). The temporal correlation with global SST indicates that both SPI and SPEI of Mozambique show a strong negative correlation with SSTs in the Central and extreme South Pacific Ocean and the Indian Ocean. In contrast, there is a strong positive correlation of SPI and SPEI with SSTs in the North and South Pacific Ocean, South Atlantic Ocean, and Antarctic Southern Ocean during months of D-J-F-M (Fig. 5i, 5j).

4.4.6. Reunion

SPI and SPEI of Reunion have a non-significant positive relationship with Nino West and a non-significant negative relationship with Nino 1+2, Nino 3, Nino 3.4, Nino 4, IOD, SIOD (Table 5). The temporal correlation with global SST delineates that both SPI and SPEI of Reunion show a strong positive correlation with SSTs in most Indian and the Pacific Ocean, including the Arctic Ocean, during months D-J-F-M (Fig. 5k, 5l).

4.4.7. Seychelles

SPI and SPEI of Seychelles have a significant negative relationship with Nino West and a non-significant positive relationship with Nino 1+2, Nino 3, Nino 3.4, Nino 4, IOD, SIOD (Table 5). The temporal correlation with global SST delineates that both SPI and SPEI of Seychelles show a strong positive correlation with SSTs in the Antarctic Southern Ocean during months of D-J-F-M (Fig. 5m, 5n).

4.4.8. South Africa

SPI and SPEI of South Africa have a significant negative relationship with Nino 1+2, Nino 3, Nino 3.4, Nino 4 and a non-significant positive relationship with Nino West, IOD, SIOD (Table 5). The temporal correlation with global SST delineates that both SPI and SPEI of South Africa show a strong negative correlation with SSTs in the Central and Extreme South Pacific Ocean and the Indian Ocean. In contrast, there is a strong positive correlation with SSTs in the North and South Pacific Ocean, South Atlantic Ocean, and Antarctic Southern Ocean during months of D-J-F-M (Fig. 5o, 5p).

4.4.9. Tanzania

SPI and SPEI of Tanzania have a significant positive relationship with Nino 3, Nino 3.4, Nino 4, and only SPEI of Tanzania has a significant negative relationship with Nino West. Also, both SPI and SPEI of Tanzania have a non-significant positive relationship with Nino 1+2, IOD, and a non-significant negative relationship with SIOD (Table 5). The temporal correlation with global SST delineates that both SPI and SPEI of Tanzania show a strong positive correlation with SSTs in the Antarctic Southern Ocean and a strong negative correlation with SSTs in a few small regions in the South Pacific Ocean months of D-J-F-M (Fig. 5q, 5r).

5. Discussion

Monthly rainfall climatology of each of the nine countries, along with the annual contribution of each of the twelve months, bring out intra- annual rainfall variability over the study region. Mostly December to March period contributes maximum rainfall of around 60% (even 73% in Mozambique) of annual rainfall. In some countries, April also contributes to good rainfall. The decadal rainfall variability has shown the multi-decadal wet and dry phases for all countries. It is also seen that negative percent departure has resulted in severe to extreme drought in some countries, including moderate droughts during positive percent departure of decadal rainfall (Nicholson S E 2001). These SWIO countries receive most of their rainfall during months of D-J-F-M, and the percent departure has shown that lack of rainfall in these months will significantly impact droughts in these countries (SWIO-RAFI, 2017).

The study presented here utilizes two drought indices, SPI and SPEI, for measuring the magnitude and severity of droughts in nine SWIO countries. SPI uses standardized precipitation only, whereas, on the other hand, SPEI uses precipitation and temperature to determine PET (Vicente-Serrano et al., 2015). In some cases, even in normal rainfall conditions, high temperature plays a crucial role in increasing evapotranspiration and thus decreasing soil moisture (Hamlet A F et al. 2007), leading to soil moisture drought. Time series analysis SPI and SPEI shows the magnitude and severity of droughts in all nine countries with multiyear droughts events at a few instances. All nine countries have experienced several moderate to severe drought episodes throughout the last century (SWIO-RAFI, 2017). Time series also shows that during the last century, Lesotho has experienced the highest number of moderate drought years, Seychelles has experienced the highest number of severe drought years, and Comoros has experienced the highest number of extreme drought years. Lesotho has also shown a significant decreasing trend of droughts. Our analysis has rightly identified the severe/extremely severe drought years over South Africa, Mozambique, and parts of Madagascar previously mentioned by Masih et al. (2014) by using Global SPEI data for the years 1991-92, 1948-49, 1972-73.

The correlation coefficients analysis for months of D-J-F-M shows that Nino 1+2, Nino 3, Nino 3.4, and Nino 4 regions have a significant negative relationship with droughts in Lesotho, Mozambique, and South Africa and a

significant positive relationship with droughts in Tanzania. Nino West has shown a significant positive relationship with droughts in Mozambique and a significant negative relationship with droughts in Seychelles. IOD has shown a significant positive relationship with droughts in Madagascar and Mozambique. SIOD has shown a significant negative relationship with droughts in Comoros and a significant positive relationship with droughts in Mozambique. Temporal correlation between global SST and SPI and SPEI of Lesotho, Mozambique, and South Africa have shown a significant negative relationship with SSTs in Central and Extreme South Pacific Ocean and the Indian Ocean, whereas SPI and SPEI of Mauritius and Reunion show a significant positive correlation with SSTs in most of the Indian and the Pacific Ocean Including Arctic Ocean. Table 5 and Figure 5 show that SPEI always shows more negative or less positive correlation coefficient than SPI with SST. This is due to the influence of potential evapotranspiration in the computation of SPEI. Lesotho is a land-locked country within South Africa, and both countries mostly show the same results for SST correlations.

6. Conclusion

The study highlights the intra-annual rainfall variability as well as decadal rainfall variability over the coastal southwest Indian ocean countries. The four months from December to March are considered the rainiest period throughout the region. Years are identified based on the drought severity with the computed drought indices. Both the drought indices are multi-scalar in nature, but the multivariate behavior of SPEI is an advantage in representing an aspect of drought. The temporal correlation showed the teleconnections between global SST and droughts in these countries, and it highlighted regions with potentially significant impact on droughts. This study also explores the effects of SSTs in the Subtropical Indian Ocean and the less known Nino West region with droughts in these southwest Indian Ocean countries. Decadal rainfall variability using percent departure rainfall delineates the multi-decadal dry and wet phases precisely.

7.Acknowledgment

The authors are thankful to the Director General of Meteorology, India Meteorological Department, for providing resources and research platform for carrying out this work. The authors are also thankful to the University of East Anglia for providing CRU TS v4.04 and to NOAA ESRL-PSL for providing COBE-SST2 dataset.

References

Behera S K and Yamagata T 2001 Subtropical SST dipole events in the southern Indian Ocean; Geophysical Research Letters 28(2) 327-330.

Beguería, S, Vicente-Serrano S M, Reig F and Latorre B 2014 Standardized precipitation evapotranspiration index (SPEI) revisited: parameter fitting, evapotranspiration models, tools, datasets and drought monitoring; International Journal of Climatology 34(10) 3001-3023.

Bouchard C, Osman S and Rafidinarivo C 2019 Southwest Indian Ocean Islands: challenges and opportunities for sustainable development, security and regional cooperation; Journal of the Indian Ocean Region 15(1) 1-7.

Giannini A 2010 The Influence of Sea Surface Temperatures on African Climate; URL: https://www. ecmwf. int/sites/default/files/elibrary/20, 12.

Gupta A K, Tyagi P and Sehgal V K 2011 Drought disaster challenges and mitigation in India: strategic appraisal; Current science 1795-1806.

Hamlet A F, Mote P W, Clark M P and Lettenmaier D P 2007 Twentieth-Century Trends in Runoff, Evapotranspiration, and Soil Moisture in the Western United States; Journal of Climate 20(8) 1468-1486.

Hua W, Zhou L, Chen H, Nicholson S E, Raghavendra A and Jiang Y 2016 Possible causes of the Central Equatorial African long-term drought; Environmental Research Letters 11(12) 124002.

Lindesay J A 1988 South African rainfall, the Southern Oscillation and a Southern Hemisphere semi-annual cycle. Journal of Climatology 8: 17–30.

M. Svoboda, M. Hayes and D. Wood 2012. Standardized Precipitation Index User Guide. World Meteorological Organization, (WMO-No. 1090), Geneva.

Man-chi W 2013 A Brief Introduction to Standardized Precipitation Index (SPI); GovHK: Hong Kong Observatory.

Masih I, Maskey S, Mussá F E F and Trambauer P 2014 A review of droughts on the African continent: a geospatial and long-term perspective; Hydrology and Earth System Sciences 18(9) 3635.

Mo K C, White G H. 1985 Teleconnections in the Southern Hemisphere; Monthly Weather Review 113(1) 22–37.

Muthige M S, Malherbe J, Englebrecht F A, Grab S, Beraki A, Maisha T R and Van der Merwe J 2018 Projected changes in tropical cyclones over the South West Indian Ocean under different extents of global warming; Environmental Research Letters 13(6) 065019.

Nicholson S E 2001 Climatic and environmental change in Africa during the last two centuries; Climate research 17(2) 123-144.

Richard Y, Fauchereau N, Poccard I, Rouault M and Trzaska S 2001 20th century droughts in southern Africa: spatial and temporal variability, teleconnections with oceanic and atmospheric conditions; International Journal of Climatology: A Journal of the Royal Meteorological Society 21(7) 873-885.

Rocha A, Simmonds I 1997. Interannual variability of south-eastern African summer rainfall. Part 1: Relationships with air-sea interaction processes. International Journal of Climatology 17: 235–265.

Ropelewski C F, Halpert M S 1987 Global and regional scale precipitation and temperature patterns associated with ElNin˜o/Southern Oscillation. Monthly Weather Review 115: 1606–1626.

Ropelewski C F, Halpert M S 1989 Precipitation patterns associated with the high index phase of the Southern Oscillation. Journal of Climate 2: 268–284.

Ropelewski C F, Halpert M S 1996 Quantifying Southern Oscillation–Precipitation relationships. Journal of Climate 9: 1043–1059.

Rowell D P 2013 Simulating SST teleconnections to Africa: What is the state of the art?; Journal of Climate 26(15) 5397-5418.

Saji, N, Goswami, B, Vinayachandran, P and Yamagata T 1999 A dipole mode in the tropical Indian Ocean. Nature 401: 360–363.

Shinoda M, Kawamura R 1996. Relationships between rainfall over semi-arid Southern Africa, geopotential heights and sea-surface temperatures. Journal of the Meteorological Society of Japan 74: 21–36.

Storch H V and Zwiers F W 1999 Statistical Analysis in Climate Research; Cambridge University Press, Cambridge 27(3) 371-373.

South West Indian Ocean risk assessment and financing initiative (SWIO-RAFI): Summary report (English). 2017. Washington, D.C.: World Bank Group.

Ting M, Kushnir Y, Seager R and Li C 2009 Forced and internal twentieth-century SST trends in the North Atlantic; Journal of Climate 22(6) 1469-1481.

Ujeneza, E L, Abiodun, B J 2015 Drought regimes in Southern Africa and how well GCMs simulate them. Clim Dyn 44, 1595–1609. https://doi.org/10.1007/s00382-014-2325-z.

Vicente-Serrano S M, Beguería S and López-Moreno J I 2010 A multiscalar drought index sensitive to global warming: the standardized precipitation evapotranspiration index; Journal of climate 23(7) 1696-1718.

Wilhite D A and Glantz M H 1985 Understanding: the drought phenomenon: the role of definitions; Water international 10(3) 111-120.

Yoshida C, Nakatsugawa M, Kudo S 2016 study on long-term water level forecasting for a river in Indonesia considering global sea surface temperature changes; Journal of Japan Society of Civil Engineers: B1 (Hydraulic Engineering) 72(4) I1-I6.